Article

Low-Temperature O$_3$ Decomposition over Pd-TiO$_2$ Hybrid Catalysts

Houcine Touati [1,*], Afef Mehri [2], Fathi Karouia [3,4], Frédéric Richard [1], Catherine Batiot-Dupeyrat [1], Stéphane Daniele [5] and Jean-Marc Clacens [1,*]

[1]   Institut de Chimie des Milieux et Matériaux de Poitiers, UMR 7285, ENSI Poitiers, Université de Poitiers-CNRS, 4 rue Michel Brunet, BP633, CEDEX, 86022 Poitiers, France; frederic.richard@univ-poitiers.fr (F.R.); catherine.batiot.dupeyrat@univ-poitiers.fr (C.B.-D.)

[2]   U.R. Matériaux et Synthèse Organique UR17ES31, Institut Préparatoire aux Etudes d'Ingénieur de Monastir, Université de Monastir, Monastir 5019, Tunisia; mehri.afef@yahoo.fr

[3]   Blue Marble Space Institute of Science, Exobiology Branch, NASA Ames Research Center, Moffett Field, CA 94035, USA; fathi.karouia@nasa.gov

[4]   Space Research Within Reach, San Francisco, CA 94110, USA

[5]   Catalyse, Polymérisation, Procédés et Matériaux, CP2M-ESCPE Lyon, UMR 5128, 43 Bld du 11 Novembre 1918, CEDEX, 69616 Villeurbanne, France; stephane.daniele@univ-lyon1.fr

*   Correspondence: touatihoucine2017@gmail.com (H.T.); jean-marc.clacens@univ-poitiers.fr (J.-M.C.)

Abstract: In aircraft and spacecraft, outside air is not directly fed to the passenger because it contains ozone at elevated altitudes. The decomposition of low concentration ozone in the air was carried out at 25 °C by catalytic oxidation on Pd-based catalysts supported on a high surface area hybrid TiO$_2$. The use of these hybrid catalysts has shown a beneficial effect, both on the catalytic activity and on the catalyst stability. Kinetic studies showed that the most promising catalytic phase (Pd/TiO$_2$_100) was the one obtained from the TiO$_2$ support containing the lowest content of citrate ligands and leading to small Pd particles (around 4 nm). The effect of catalyst synthesis on the decomposition of O$_3$ gas (15 ppm) in a dry and humid (HR = 10%) stream in a closed environment such as aircraft or spacecraft was also investigated in this study and further elucidated by detailed characterizations. It was shown that the system could be used as an effective treatment for air coming from outside.

Keywords: ozone decomposition; Pd-based catalyst; TiO$_2$ hybrid support

1. Introduction

Human activity in various industrial sectors can be considered the main cause of air pollution that leads to the presence of gaseous air pollutants such as CO, O$_3$, NO$_2$, and SO$_2$ [1,2]. Ozone is considered to be a secondary air pollutant with environmental and human toxicity [3–6]. It results from complex photochemical reactions between different pollutants such as nitrogen oxides (NO$_x$), carbon monoxide (CO), volatile organic compounds (VOCs) (fuels, paints, manufacturing facilities, etc.), and sunlight [7]. However, at low concentrations, ozone is corrosive, strongly oxidizing, and toxic to human health [8–10]. Thermodynamically, ozone is an unstable gas (at 298 K ΔrG° = -163 kJ mol^{-1} and ΔrH° = -138 kJ mol^{-1}).

It forms naturally in the stratosphere, forming the protective layer of ozone around 20 km altitude, by a photochemical phenomenon involving oxygen and UV radiation [8,11].

The U.S. Environmental Protection Agency (EPA) fixed the outdoor ozone levels at 0.08 ppm for 8 h. The Food and Drug Administration (FDA) requires ozone output from indoor medical devices to be less than 0.05 ppm, but short-term exposures to ozone at levels below international standards also result in an increased risk of death [12].

In this context, long-term exposure to high concentrations of ozone can cause serious damage to the health of passengers in airplanes or astronauts in spacecraft during their travels or missions [13–16].

Various solutions to reduce pollutant concentrations were proposed, such as heterogeneous photocatalysis, [17–19] thermal, and catalytic decomposition at high temperatures [20–23].

For example, in airplanes and spacecraft, outside air is not directly supplied to passengers because it contains a high concentration of ozone at high altitudes [23,24]. Catalytic converters are hence needed to lower ozone concentrations to the authorized values. Such onboard equipment already exists but must evolve to be adapted to future aircraft and spacecraft technologies and will require working at much lower temperatures and in the presence of lower relative humidity. In the decomposition of ozone, the use of catalysts based on transition or noble metals alone, or supported on oxides, is the most widely used process because it allows high efficiency and low energy consumption [8–10,25–27]. Moreover, in the literature [12], catalysts based on manganese and palladium are known to be effective in the reaction of the decomposition of this trioxygen (O_3) molecule [28–31]. Likewise, previous studies have been performed in a temperature range between 20 and 100 °C and O_3 concentrations between 5 and 1600 ppm. In addition, various parameters can influence the performance of catalysts used, such as sulfur, NO_x, humidity, ozone concentration, and temperature [8,11]. An important specific surface area and small size of metal nanoparticles have been shown to achieve very high efficiency in the decomposition of ozone [17,32]. In addition, among the catalysts, palladium supported on titanium dioxide presents an important challenge for the O_3 decomposition because of its large specific surface area and the synthesis method [17,18]. In this study, we developed new Pd-based heterogeneous catalysts for the decomposition of ozone. For this purpose, titania-supported palladium nanoparticles by one-pot deposition method using citrate-functionalized TiO_2 hybrid support nanomaterials were investigated [33,34].

Functionalization of the titanium oxide surface by citrate (Cit) groups could provide active centers for (i) the selective Pd deposition, (ii) "in situ" reduction, and (iii) control of the growth step of Pd nanoparticles (NPs). At room temperature, different Cit/Ti molar ratios were evaluated in the decomposition of ozone under very specific conditions (low concentration of the order of 15 ppm, relative humidity of the order of 10%) and close to the real conditions for the elimination of this molecule in the cabins of planes and spacecraft.

2. Results and Discussion

2.1. Catalysts Synthesis

The catalysts were synthesized in two major steps, the first one consisting in hydrolyzing, via the Sol–Gel process, a mixture of $Ti(O^iPr)_4$, and a heteroleptic alkoxide precursor of general formula $[Ti(OiPr)_x(Cit)_y]_m$ to obtain TiO_2 nanoparticles surface functionalized by citrate ligands. Depending on the initial citrate/Ti molar ratio (x), a series of hybrid nano-objects $(Cit)_1(TiO_2)_x$ (x = 20; 50 and 100) with controlled surface citrate density are obtained. These latter are used as a reduction site in a second step to deposit Pd nanoparticles (PdNPs) on TiO_2. A mild thermal treatment (70 °C under air) is finally applied to clean the surface from any residual solvent.

2.2. Physicochemical and Morphological Properties of Catalysts

The properties of catalysts were first assessed by in situ ATR-IR. Results of the Pd/TiO_2_x catalysts have shown similar profiles to those of the supports alone $((Cit)_1(TiO_2)_x)$ (Figure 1) with bands at 1620 cm^{-1} and 1380 cm^{-1} that were attributed to the presence of carboxylate groups COO^- [35]. The bands due to stretching vibrations ν (C=O) groups of citric acid (at 1735 cm^{-1} and 1710 cm^{-1}) were not detected, indicating the presence of higher $TiO_2\_citrate$ interactions.
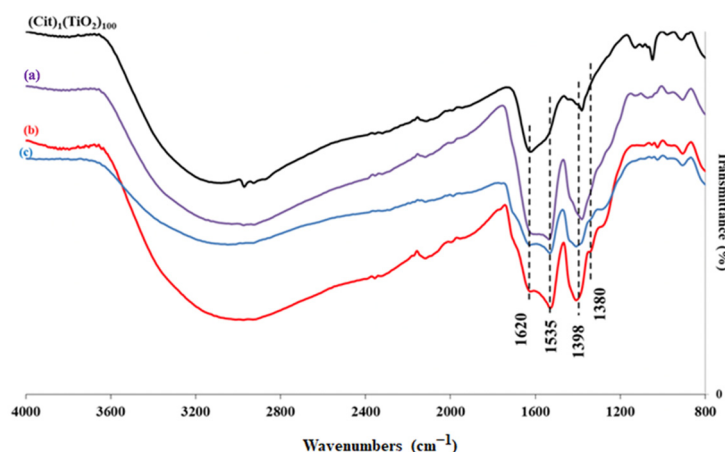
Figure 1. ATR-IR spectra of $(Cit)_1(TiO_2)_{100}$ and (a) Pd/TiO_2_20, (b) Pd/TiO_2_50, and (c) Pd/TiO_2_100 catalysts after drying at 70 °C for 24 h.

The characteristic vibrations of the inorganic TiO_2: Ti-O-Ti (1120 cm^{-1}) and Ti-O (962 and 720 cm^{-1}) [36] did not change, showing that the inorganic structure of TiO_2 was not impacted by the presence of citric acid. After palladium deposition, the ATR-IR spectra showed the disappearance of the band relative to νCOO^- located at 1385 cm^{-1}. For all catalysts (Pd/TiO_2_x), two new vibration bands situated at 1535 and 1398 cm^{-1} were observed, suggesting that the deposition of Pd allows modifying the citrate coordination on the TiO_2 surface since a higher proportion of bridged moieties after Pd deposition was observed. This result would be in agreement with the presence of a strong interaction of the carboxylic groups of citrates with Pd.

ICP-AES analyses for different catalysts are summarized in Table 1. Irrespective of the catalyst, the amount of palladium deposited was close to the desired value (0.40 wt%). Moreover, the percentage of Pd fixed on the various hybrid supports $(Cit)_1(TiO_2)_x$ seemed to be related to the quantity of citrate present. Indeed, in the presence of a high citrate content in the hybrid support (Pd/TiO_2_20), the quantity of Pd measured (0.40 wt%) is the one excepted. A decrease in citrate in the support led to a decrease in the amount of Pd deposited (0.32% of Pd in Pd/TiO_2_100), suggesting that the amount of citrate on the TiO_2 surface is not sufficient to reduce the amount of palladium initially introduced (0.40%).

Table 1. Pd loading (ICP-AES) and XPS results for the Pd/TiO_2_x (x = 20, 50, 100) and $Pd/TiO_2\_$citrate free catalysts.

Catalyst	Pd [a] (wt%)	Pd $3d_{5/2}$ (XPS) Pd°/PdO$_x$ (%)	Pd (at.%)	Pd/Ti (XPS)	O (%)	N [b] (%)	C [b] (%)
Pd/TiO_2_20	0.40	75/25	0.05	0.0033	52	0.04	23.83 (4.80)
Pd/TiO_2_50	0.36	71/29	0.08	0.0044	57	0.02	19.60 (3.04)
Pd/TiO_2_100	0.32	70/30	0.10	0.0062	58	0.01	17.05 (1.80)
$Pd/TiO_2\_$citrate free	0.39	nd/nd		nd	nd	nd	nd

[a] determined by elemental analysis (ICP-AES); [b] determined by CHNS analysis.

The isotherms of adsorption–desorption of N_2 of all Pd-based catalysts were of type IV, according to the IUPAC classification (Figure 2). The presence of hysteresis suggested a mesoporosity of the surface of the studied materials in which a capillary condensation occurred. After functionalization with citrate precursors, the hysteresis loop extended over a relatively wide range of relative pressures; at P/P° values between 0.40 and 0.47, this decrease could be related to the increase in the Ti/Cit ratio. This value was higher (close to 0.54) for $Pd/TiO_2\_$free citrate. The results for the measurements of specific surface area (S_{BET}), pore volume (Vp), and average pore diameter (Dp) of the catalysts prepared in the presence and absence of citrate precursors are given in Table 2.
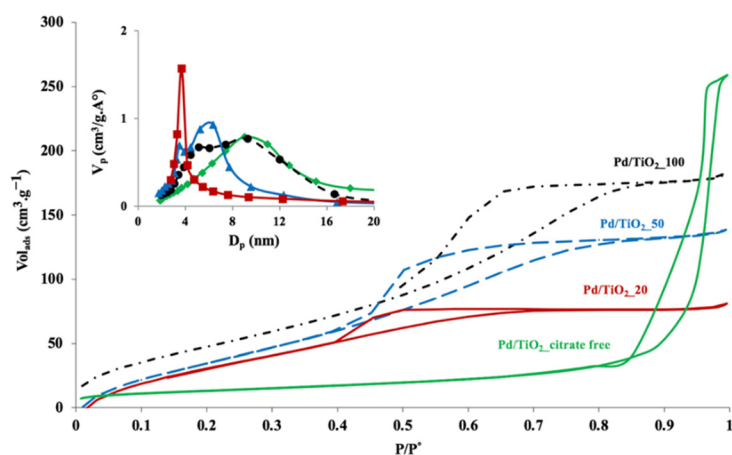
Figure 2. N2 adsorption–desorption isotherms and pore size distribution of Pd/TiO2_x (x = 20, 50 and 100) and Pd/TiO2_citrate free catalysts.

Table 2. Surface areas and nanoparticles size for the Pd/TiO$_2$_x (x = 20, 50, 100) and Pd/TiO$_2$_citrate free catalysts.

Catalyst	S$_{BET}$ (m^2 g^{-1})	D$_p$ (nm)	Vp (cm^3 g^{-1})	C$_{BET}$ [a]	d$_{XRD}$ (nm)	d (nm) [b]
Pd/TiO$_2$_20	279 (335)	25 (25)	0.18 (0.13)	116 (116)	5.0 (6.0)	6
Pd/TiO$_2$_50	268 (303)	35 (33)	0.20 (0.19)	72 (71)	6.0 (6.5)	3
Pd/TiO$_2$_100	223 (263)	70 (75)	0.31 (0.29)	70 (70)	6.5 (7.0)	4
Pd/TiO$_2$_citrate free	232 (212)	65 (65)	0.49 (0.40)	103 (109)	9.0 (8.5)	12

[a]—he BET constant. [b]—Pd Nanoparticles size determined by TEM. ( )—value for Pd free support.

Interestingly, all the modified titanium oxides exhibited higher S$_{BET}$ specific surfaces, lower pore volumes (Vp), and smaller pore sizes than Pd/TiO$_2$_citrate free. The low values of the C$_{BET}$ constant confirmed that the -COOH groups were located on the surface of titanium oxide particles. BET surface areas increased with increasing citrate content; hence a higher value was obtained for the highly functionalized material TiO$_2$_20 exhibiting a surface area of 335 m^2 g^{-1}. This was consistent with the presence of an important amount of surface organic functionalization, which could induce self-assembly of the nanocrystallites and create extra mesoporosity, as evidenced by the N$_2$ adsorption–desorption isotherm (Figure 2).

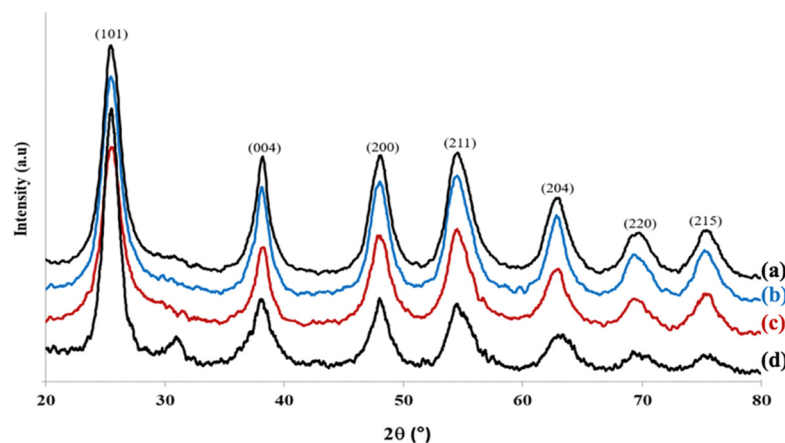The XRD patterns of the different catalysts are shown in Figure 3.

Figure 3. XRD patterns of Pd/TiO$_2$_x catalysts: (a) x = 100; (b) x = 50; (c) x = 20; (d) Pd/TiO$_2$_citrate free after drying at 70 °C for 24 h.

All functionalization materials exhibited the anatase phase. The material containing the largest amount of citrate also displayed the poorest crystallinity, showing that a significant amount of citrate on the surface resulted in a disruption of the crystal lattice. After reductive deposition of nanoparticles of Pd and compared with the supports, the crystallinity of TiO_2 anatase did not change (JCPDS card no.21-1272). Moreover, the metallic Pd phase was never detected in the XRD diffractograms, which may come from the small amount of deposited Pd but also indicates a good dispersion of Pd nanoparticles on the surface of TiO_2.

Analysis of the XPS spectra of Pd $3d_{5/2}$ showed the presence of two contributions corresponding, respectively, to metallic Pd° and PdO_x species (Figure 4). Binding energies for $3d_{5/2}$ and $3d_{3/2}$ appeared at 334.3 eV and 339.6 eV for Pd° and 336.1 eV and 341.4 eV for PdO_x, respectively [37,38]. In addition, the presence of citrate species favored the reducibility of Pd. The amount of reduced palladium (Pd°) increased as the Cit/Ti ratio increased: 75% of Pd° using $(Cit)_1(TiO_2)_{20}$ versus 70% using $(Cit)_1(TiO_2)_{100}$ as support (Table 1). In contrast, the Pd/Ti atomic ratio tended to decrease when increasing the citrate content from x = 100 to 20. This suggests that too high citrate content can lead to a depleted dispersion of Pd onto the TiO_2 surface and the entrapment of a non-negligible fraction of Pd inside the TiO_2 support (Table 1).

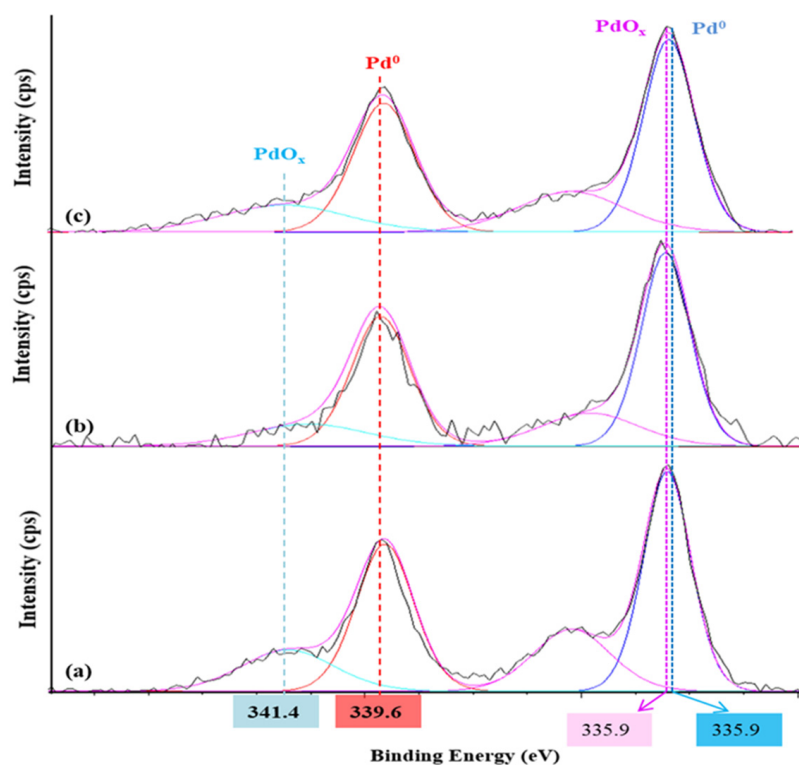**Figure 4.** Pd_{3d} XPS Spectra of Pd/TiO_2_x: (**a**) x = 20; (**b**) =50, and (**c**) =100 after drying at 70 °C for 24 h.

The size distributions of Pd nanoparticles (PdNPs) prepared using different $(Cit)_1(TiO_2)_x$ supports, obtained by TEM analysis, are shown in Figure 5. TEM micrographs showed that the produced PdNPs were of spherical shape with an average size between 3 and 7 nm (Table 2).
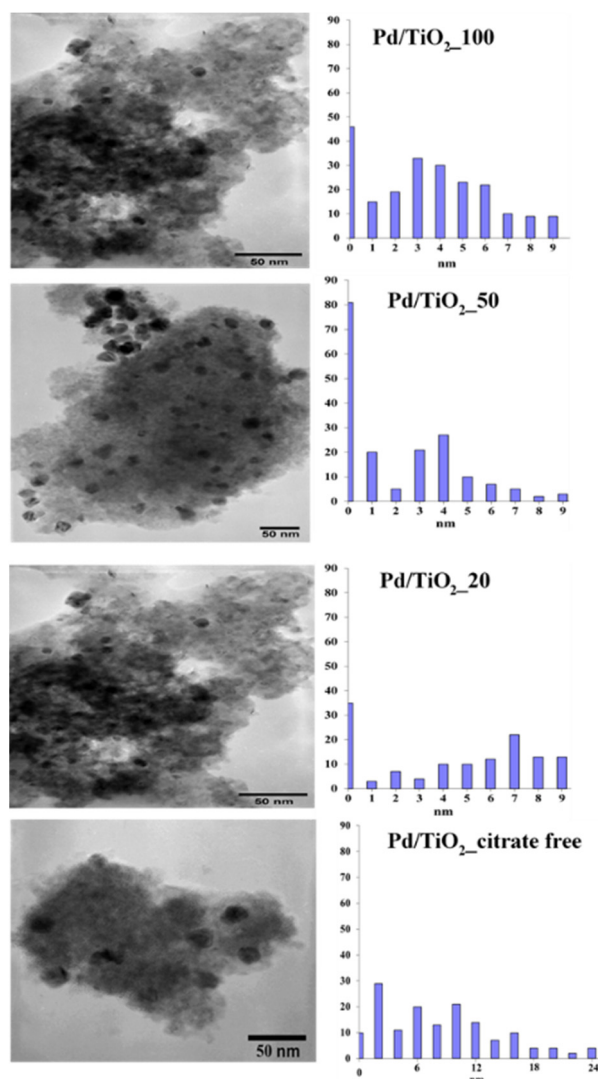
Figure 5. TEM pictures of the Pd/TiO$_2$_x (x = 20, 50, and 100) catalysts and Pd/TiO$_2$_citrate free after drying at 70 °C for 24 h.

This result confirmed the reducing effect of the carboxylate groups of the citrates in agreement with ATR-IR results. Citrate amounts seemed to have an impact on the diameter distribution of palladium nanoparticles. It is interesting to note that PdNPs prepared from (Cit)1(TiO$_2$)$_{50}$ have the smallest mean diameter, which is 3 ± 0.8 nm. By increasing the citrate amount (x = 20), the PdNPs had a mean diameter of 6 nm and showed a broader size distribution than (Cit)$_1$(TiO$_2$)$_{50}$ and (Cit)$_1$(TiO$_2$)$_{100}$ supports (Figure 5). This result could be explained by the agglomeration of very small particles of Pd, in agreement with the results reported by Y. Sun et al. [39]. Indeed, a higher concentration of citrate could generate the appearance of more Pd nuclei at the same place and thus favor the growth of Pd nanoparticles.

2.3. Catalytic Properties

2.3.1. Effect of Pd Free Support on O$_3$ Decomposition

The results of the decomposition of ozone on the different synthesized and commercial TiO$_2$ supports (TiO$_2$_citrate free, used as reference) under dry and humid conditions at 25 °C have been presented in Figure 6. For all supports, a transient decrease in ozone conversion efficiency occurred systematically initially (for about 1 h) until stabilization of the ozone conversion (at around 20% on TiO$_2$_citrate free). All hybrid TiO$_2$ materials exhibited higher activity in ozone decomposition than TiO$_2$_citrate free. This efficiency

could be partly explained by a modification of the textural properties of these TiO_2 hybrid materials since their specific surface area (between 263–335 m^2 g^{-1}) was much larger than the one of TiO_2_citrate free (232 m^2 g^{-1}). Regardless of the solid, the presence of water (in presence of humid air) led to a decrease in the ozone conversion compared with experiments carried out in the presence of dry air. As an example, the ozone conversion was close to 30% under dry air on $(Cit)_1(TiO_2)_{100}$ and equal to 23% when humid conditions were used.
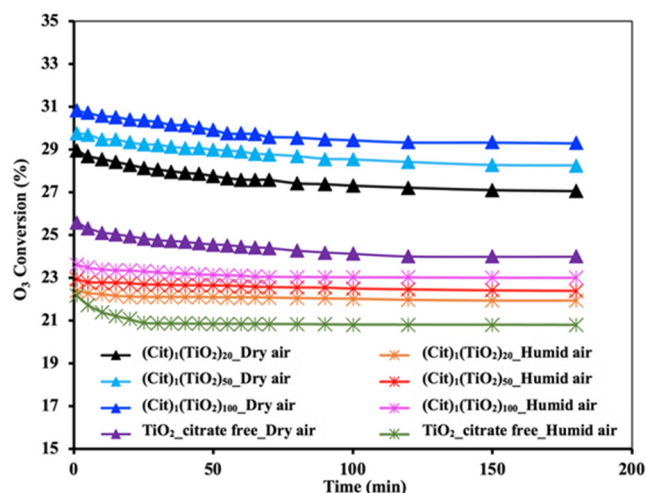

Figure 6. Ozone conversion as a function of time on stream in dry and humid conditions for the Pd free hybrid support (x = 20, 50, 100) and TiO_2_citrate free reference. (Experimental conditions: catalyst = 10 mg, O_3 = 15 ppm, H_2O = 3130 ppm (corresponding to RH = 10%), flow rate = 1000 mL min^{-1}, T = 25 °C).

2.3.2. Catalytic Activity in Dry and Humid Conditions

Under humid conditions (RH = 10%), a strong inhibiting effect of water was observed on ozone conversion for support only ($(Cit)_1(TiO_2)_x$ (x = 20, 50 and 100) and TiO_2_citrate free) (Conversion (%) = 20–24) (Figure 6).

However, the addition of palladium remarkably improved the efficiency of these nanomaterials in the decomposition of O_3 under both dry and humid conditions (Figure 7a,b), indicating the beneficial effect of palladium on the limitation of decreasing O_3 decomposition (Conversion (%) = 40–100) [8,24].

These results show that impregnating Pd can promote the conversion of O_3 very effectively for humid and dry ozone gas mixtures. Independently of the hybrid-supported Pd-based catalyst used, the ozone conversion was between 76% and 100% after 3 h of reaction under dry and humid conditions. On the other hand, a significant influence of the nature of the support was noticed in both conditions. The catalysts based on hybrid TiO_2 showed higher efficiency for ozone decomposition compared with Pd/TiO_2_citrate free. Indeed, Pd/TiO_2_100 as a catalyst allowed obtaining a total conversion of ozone with or without dry air, whereas the ozone conversion determined over Pd/TiO_2_citrate free after 180 min of reaction time was close to 40% under dry and 21% under humid air. The beneficial effect could be attributed to a better dispersion of Pd on the surface of TiO_2 because of the presence of a citrate group at the surface of the different supports. Indeed, according to XPS and TEM results, the catalyst containing the lowest citrate content (Pd/TiO_2_100) exhibited Pd nanoparticles with an average diameter of about 4 nm. By increasing the amount of citrate, the particle size was also increased to 6 nm, causing a decrease in O_3 conversion (Pd/TiO_2_20). Therefore, the small size of Pd nanoparticles appeared to increase the conversion of ozone to oxygen at the surface of the catalyst.
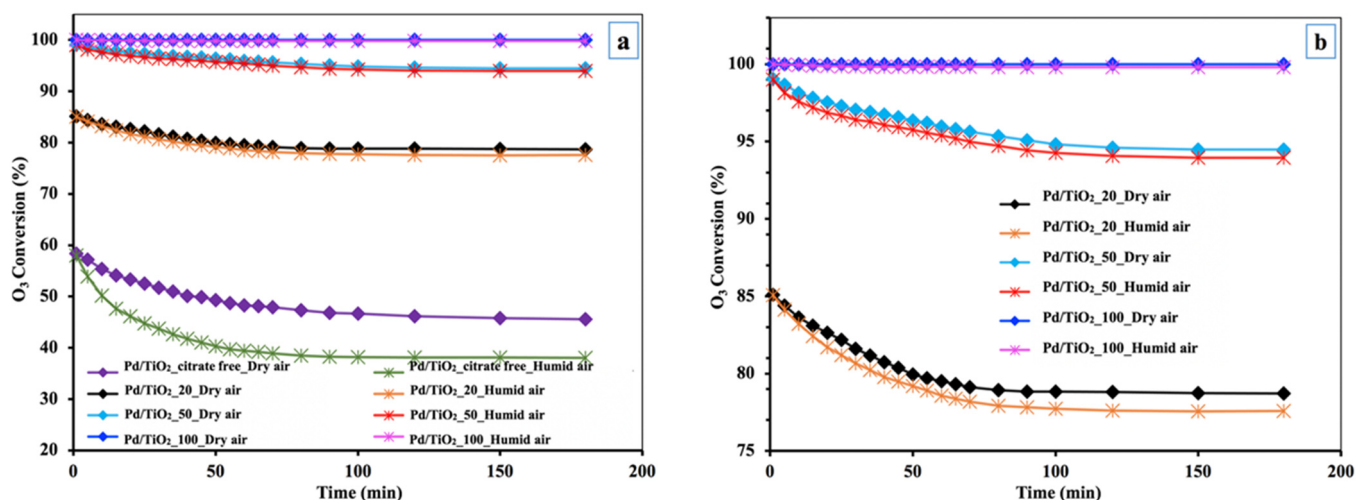
Figure 7. (**a**) Ozone conversion as a function of time on stream in dry and humid conditions for the Pd/TiO$_2$_x (x = 20, 50, 100) and Pd/TiO$_2$_citrate free catalysts. (Experimental conditions: catalyst = 10 mg, O$_3$ = 15 ppm, H$_2$O = 3130 ppm (corresponding to RH = 10%), flow rate = 1000 mL min^{-1}, T = 25 °C). (**b**) Enlargement of (**a**) in the 75–100% conversion range.

On all Pd supported on hybrid supports, the TOF values were always between 1.7 and 2.5 times higher than over Pd/TiO$_2$_citrate free (Table 3). However, considering their respective Pd loadings and particle sizes as determined by BET and TEM, TOF calculations showed that the intrinsic activities of the Pd supported on hybrid supports (Pd/TiO$_2$_20, Pd/TiO$_2$_50, and Pd/TiO$_2$_100) and Pd/TiO$_2$_citrate free catalysts were really different reaching values around 135.1 min^{-1} for Pd/TiO$_2$_citrate free and 235.4–348.7 min^{-1} for Pd/TiO$_2$_x in dry conditions.

Table 3. TOF values of different Pd/TiO$_2$_x (x = 20, 50, 100) and Pd/TiO$_2$_ citrate free catalysts under dry and humid conditions.

	TOF (min^{-1})	
Catalyst	**Dry**	**Humid**
Pd/TiO$_2$_20	235	235
Pd/TiO$_2$_50	306	304
Pd/TiO$_2$_100	349	349
Pd/TiO$_2$_citrate free	142	130

Under humid conditions (RH = 10%), a decrease in ozone conversion efficiency was observed for the Pd/TiO$_2$_citrate free catalyst indicating a strong inhibiting effect of water on the decomposition of ozone. This phenomenon was highlighted by a drop in TOF (>10%). On the other hand, the TOF values were not really very different (<0.5%) for Pd supported on hybrid supports, indicating that the presence of citrate decreased the water impact and thus highlighted the beneficial effect of the presence of citrate moieties on the catalytic properties of Pd supported on hybrid materials. The positive effect of palladium in limiting the decrease in ozone decomposition in the presence of water has already been observed [13,40–43], although several authors did not observe the inhibitory effect of water vapor [9,10,27,44,45]. This difference could be explained by the presence of NO$_x$ inside the reactor when the air was used instead of oxygen to generate ozone [46].

Indeed, the effect of water has been shown to be limited in the presence of NO$_x$, as demonstrated by Subrahmanyam et al. on activated carbon [46] and Mehandjiev et al. on catalysts based on manganese oxide [47–49]. However, the addition of a small amount of palladium was found to considerably limit this undesirable effect. It has been proposed that the inhibiting effect of water was not due to a surface modification of the catalyst

but rather to the blocking of active sites responsible for ozone decomposition by water adsorption [41,50]. If NO_x species were produced in the gas stream, adsorbed water could react with them to form nitric or nitrous acid and hence limit the negative effect of water [11]. This would result in the removal of water and gas phase NO_x species and the release of sites for ozone reaction. The role of palladium could be favored by electron transfer to titanium, which contributed to the desorption of water from titanium cations [40,41,51]. The stability of such catalysts could be explained by the presence of Pd, which is well-known for its high efficiency in oxidation reactions; on the other hand, the citrate-modified TiO_2 supports, rich in OH groups, as is known by a large specific surface area, has an important effect also in this capacity of decomposition of O_3.

2.3.3. Effect of the Catalyst Weight in the O_3 Decomposition

The amount of the catalyst is an important parameter because it determines the ozone decomposition capacity under operating conditions. As expected, the increase in catalyst quantity led to an increase in ozone decomposition both in dry and humid air (Figure 8).
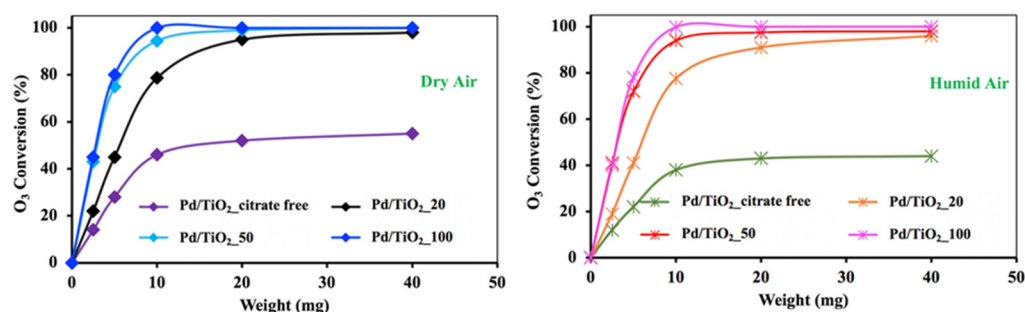

Figure 8. Effect of catalyst mass on ozone conversion for Pd/TiO_2_x (x = 20, 50, 100) and $Pd/TiO_2\_$citrate free catalysts. (Experimental conditions: m = 2.5; 5; 10; 20 and 40 mg, O_3 = 15 ppm, H_2O = 3130 ppm (corresponding to RH = 10%), flow rate = 1000 mL min^{-1}, T = 25 °C).

Above 20 mg of catalyst, full ozone conversion was noticed whatever the Pd supported on hybrid supports. For $Pd/TiO_2\_$citrate free, the conversion of ozone seemed to be limited to 52% conversion in dry air and 43% in the humid air.

3. Materials and Methods

3.1. Materials

Titanium isopropoxide ($Ti(O^iPr)_4$, 99.99%), Isopropanol (HO^iPr, 99.7%), THF ($C_4H_8O.H_2O$, 99.9%), $NaBH_4$ (98%), Na_2PdCl_4 (99.99%), and citric acid ($C_6H_8O_7.H_2O$, 99.5%) were purchased from Aldrich. The tetra-n-butyl-ammonium bromide (NBu_4Br, 99%) was obtained from Acros.

3.2. Catalyst Preparation

3.2.1. Preparation of Hybrid $(Cit)_1(TiO_2)_x$ (x = 20; 50 and 100)

The hybrid titanium oxide synthesis method used was described previously [33]. Under argon, 1.06 mL of titanium isopropoxide $Ti(O^iPr)_4$ and 248 mg of citric acid (Ti: Cit molar ratio = 3) were added to 10 mL of THF. The medium was kept under vigorous stirring for 16 h. The ^{13}C NMR analysis of the mixture shows the formation of the $Ti_3O(O^iPr)_8(OOCCH_2$-$C(OH)(COO)$-$CH_2COOH)$ complex. Then, 10 mL of isopropanol (HO^iPr) and (x−3) equivalent mol of $Ti(O^iPr)_4$, regarding to citrates, were added to the complex allowing to obtain three hybrid supports with various Ti/Cit ratios (20, 50, and 100). This solution was added to 0.1 equivalents of NBu_4Br in 100 mL of distilled water in a two-necked flask maintained under reflux at 100 °C. The suspensions were heated under reflux for 3 h. The precipitate was then washed twice with water and once with ethanol and finally dried at 70 °C for 20 h.

3.2.2. Preparation of TiO$_2$_Citrate Free

The same method was used as described in Section 3.2.1 without using citric acid. The support is used as a reference.

3.2.3. Preparation of Pd Supported on Hybrid TiO$_2$

(a) Preparation of 0.4%Pd/(Cit)$_1$(TiO$_2$)$_x$ catalysts (Pd/TiO$_2$_x).

The Pd/(Cit)$_1$(TiO$_2$)$_x$ catalysts were prepared by a reductive deposition method described by Mehri et al., using surface citrate as the reducing agent [34]. Typically, to 100 mL H$_2$O containing 0.01 mmol of palladium (Na$_2$PdCl$_4$-0.4%*w/w*), the desired (Cit)$_1$(TiO$_2$)$_x$ support (250 mg) was introduced. The suspension is stirred at 100 °C for 3 h. The catalysts were recovered after 3 washes with water and dried at 70 °C overnight. These solids were noted as Pd/TiO$_2$_20, Pd/TiO$_2$_50 and Pd/TiO$_2$_100, depending on the value of x.

(b) Preparation of 0.4%Pd/TiO$_2$_citrate free catalysts (Pd/TiO$_2$_citrate free).

Pd was deposited on TiO$_2$-citrate free from an aqueous solution of Na$_2$PdCl$_4$ by simple impregnation: 0.01 mmol (5 mL) of Pd was mixed with 250 mg of support. Then, this catalyst was reduced by an aqueous solution of NaBH$_4$ (0.1 mmol), washed with distilled water, and dried at 70 °C.

3.3. Characterization Methods

X-ray powder diffractograms were obtained using an Analytical XPERTMPD Pro diffractometer using Cu Kα radiation (λ = 1.542 Å). The Pd loading amount in the catalysts was determined by inductively coupled plasma–atomic emission spectroscopy (ICP-AES) using the Horiba Jobin Yvon instrument. The morphology of Pd nanoparticles was characterized by transmission electron microscopy higher resolution (HR-TEM) with a JEOL 2010 instrument equipped with EDX capabilities. The size and size distribution of Pd were determined using Sigma Scan Pro.5 software. N$_2$ adsorption-desorption isotherms at 77 K were performed using a Micromeritics ASAP 2010 instrument. The Brunauer–Emmett–Teller (BET) equation was used to calculate the specific surface area (S$_{BET}$). The infrared absorption spectra of the synthesized products were recorded using a PerkinElmer Paragon 500 FT-IR spectrometer using a diamond/ZnSe ATR crystal in the region of 4000 to 400 cm^{-1}. Chemical states of the palladium and carbon in the catalyst surface were investigated by X-ray photoelectron spectroscopy (XPS) on an Axis Ultra DLD (Kratos Analytical) equipped with a dual Al/Mg anode. The spectra were obtained using the Al Kα source (1486.6 eV). All spectra were measured between 0 and 1200 eV pass energy. The constant charging of the different catalysts was corrected by referencing all the energies to the C$_{1s}$ peak at 284.6 eV arising from adventitious carbon. Elemental carbon analysis is determined using a brand CHNS elemental analyzer Horiba Jobin Yvon model EMIA 220 V.

3.4. Catalytic Test

The catalytic activity tests were carried out in a conventional flow reactor under atmospheric pressure at 25 °C. The composition of the reacting gas flow was 15 ppm of O$_3$ in 1000 mL min^{-1} of air. Various amounts of powder catalyst (2.5, 5, 10, 20, or 40 mg) were used.

Ozone was generated with a homemade apparatus by flowing pure oxygen through a nonthermal plasma reactor, the existing ozone–oxygen mixture was diluted by air. Water was introduced into the gas flow by bubbling a part of the airflow in a saturator-type vessel containing water prior to being mixed with ozone–air mixture to obtain the humid conditions. The amount of water was fixed by controlling the temperature of the saturator by a cryostat. The relative humidity was fixed at 10%, which corresponds to 3130 ppm of water introduced in the gas flow at 25 °C. Ozone was analyzed by an ozone analyzer (Environment S.A., type "O$_3$ 42 M") based on the UV photometric method at 254 nm [8].

Our analytical system is presented in Figure 9, and ozone concentration was chosen according to the reaction of ozone activation on a catalyst:
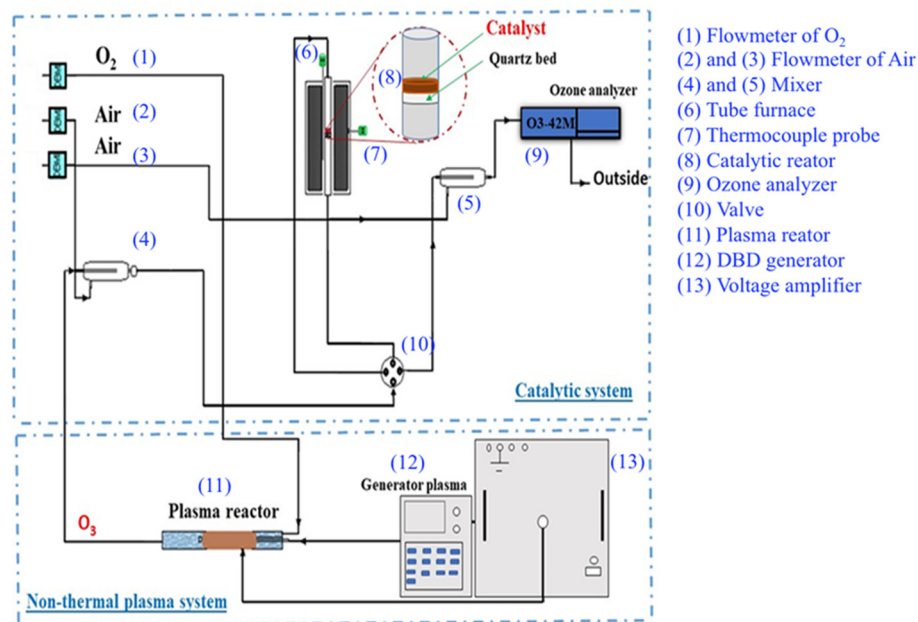
$$O_3 = O_2 + O * \tag{1}$$

Figure 9. Experimental setup to decompose O_3 at 25 °C.

The percentage of a converted chemical species (O_3) is expressed by the ratio between the amount of consumed reagent and the initial amount of reagent.

$$\text{Conversion of ozone: } XO_3\,(\%) = 100 \times (\text{conc } O_{3i} - \text{conc } O_{3f})/\text{conc } O_{3i}$$

With conc O_{3i}: the inlet concentration of ozone;
With conc O_{3f}: the outlet concentration of ozone.

Turnover frequencies (s^{-1}) are defined as the number of moles of O_3 converted per number of moles of surface Pd atoms per second; they are determined as follows:

$$\text{TOF} = \frac{Y_{O3} * X_{O3} * V_{gas} * M_{Pd}}{m_{Pd} * d} \cdot (s^{-1})$$

where:

- mPd is the mass of Pd in the catalytic (g);
- Vgas is the total molar flow rate (=$1000/(60 \times 22,400)$) = 7.5×10^{-4} mol·s^{-1};
- X_{O3} is conversion of O_3;
- Y_{O3} is the mole fraction of O_3 in the in-let gas mixture (80% Ar/20% O_2);
- M_{Pd} is the molecular weight of Pd (106.42 g·mol^{-1});
- d is the dispersion of the Pd particles determined by the dynamic pulsed hydrogen chemisorption technique.

Gas hourly space velocity was calculated considering a catalyst density of 4 g·mL^{-1}. So, for 2.5 mg of catalyst, we obtain a GHSV of $60{,}000/0.0025 \times 4 = 96 \times 10^6$ h^{-1} and, for 40 mg, a GHSV of 6×10^6 h^{-1}.

4. Conclusions

Ozone decomposition was studied at 25 °C on Pd catalysts with various textural properties, as well as supported on citrate-modified TiO_2 under dry and humid conditions. This study clearly showed the importance of surface citrate in the reduction of palladium

nanoparticles on the surface of TiO_2. Depending on the Ti/Cit molar ratio, the particle size of the Pd nanoparticles could be controlled, greatly modifying the activity properties by modifying the electronic properties of the final Pd/TiO_2_x catalysts. Compared with $TiO_2\_$citrate free, highly intrinsically active Pd/TiO_2_x catalysts could be obtained for the decomposition of ozone. These citrate groups on the support surface have shown great persistence to water vapor.

First of all, the activities of the hybrid supports $(Cit)(TiO_2)_x$ (x = 20, 50, 100) and $TiO_2\_$citrate free were slightly decreased at the beginning of the reaction and then became stable under dry conditions. However, in the presence of humidity, the activity was clearly sensitive to the presence of water vapor for all supports (around an 8% decrease). The TiO_2_100 hybrid support, with the lowest amount of citrate, showed a significantly higher efficiency compared with the reference $TiO_2\_$citrate free support, as well as hybrid supports richer in citrate.

The Pd-doped TiO_2_x supports were very active in the O_3 decomposition reaction, whatever the operating conditions (humid or dry air catalytic tests). This showed that the presence of Pd had a very beneficial effect in the presence of water vapor. In contrast, the low citrate catalyst (Pd/TiO_2_100) was very efficient in both the wet and dry air reactions. We have also shown that this catalyst was more effective regardless of the amount of material used for 3 h of reaction. This efficiency was explained by the particle size of Pd, which was smaller for Pd/TiO_2_100 compared with Pd/TiO_2_20. Thus, the total elimination of 15 ppm of ozone by this catalytic system under specific experimental conditions (residence time lower than 1.38 ms) allows us to envisage this method for treating indoor and outside air in different settings that could be beneficial to human health and environmental factors.

Author Contributions: Conceptualization, H.T., S.D., J.-M.C., C.B.-D.; methodology, J.-M.C., S.D., H.T.; validation, J.-M.C., S.D., C.B.-D., F.K.; formal analysis, H.T., A.M., J.-M.C., S.D., C.B.-D.; data curation, H.T.; visualization, H.T., A.M., F.K., F.R., S.D., C.B.-D., J.-M.C.; writing—original draft preparation, H.T., A.M., J.-M.C.; writing—review and editing, H.T., A.M., S.D., F.R., J.-M.C.; supervision, J.-M.C., S.D., C.B.-D.; project administration, J.-M.C.; funding acquisition, J.-M.C. and S.D. All authors have read and agreed to the published version of the manuscript.

Data Availability Statement: Not applicable.

Conflicts of Interest: The authors declare no conflict of interest.

References

1. Wang, X.-C.; Klemeš, J.J.; Dong, X.; Fan, W.; Xu, Z.; Wang, Y.; Varbanov, P.S. Air pollution terrain nexus: A review considering energy generation and consumption. *Renew. Sustain. Energy Rev.* **2019**, *105*, 71–85. [CrossRef]
2. Touati, T.; Valange, S.; Reinholdt, M.; Batiot-Dupeyrat, C.; Clacens, J.-M.; Tatibouët, J.-M. Low Temperature Catalytic Oxidation of Ethanol Using Ozone over Manganese Oxide-Based Catalysts in Powdered and Monolithic Forms. *Catalysts* **2022**, *12*, 172. [CrossRef]
3. Yue, X.; Unger, N.; Harper, K.; Xia, X.G.; Liao, H.; Zhu, T.; Xiao, J.F.; Feng, Z.Z.; Li, J. Ozone and Haze Pollution Weakens Net Primary Productivity in China. *Atmos. Chem. Phys.* **2017**, *17*, 6073–6089. [CrossRef]
4. Fann, N.; Lamson, A.D.; Anenberg, S.C.; Wesson, K.; Risley, D.; Hubbell, B.J. Estimating the National Public Health Burden Associated with Exposure to Ambient $PM_{2.5}$ and Ozone. *Risk Anal.* **2012**, *32*, 81–95. [CrossRef]
5. Cohen, A.J.; Brauer, M.; Burnett, R.; Anderson, H.R.; Frostad, J.; Estep, K.; Balakrishnan, K.; Brunekreef, B.; Dandona, L.; Dandona, R.; et al. Estimates and 25-year trends of the global burden of disease attributable to ambient air pollution: An analysis of data from the Global Burden of Diseases Study 2015. *Lancet* **2017**, *389*, 1907–1918. [CrossRef]
6. Anenberg, S.C.; Schwartz, J.; Shindell, D.; Amann, M.; Faluvegi, G.; Klimont, Z.; Janssens-Maenhout, G.; Pozzoli, L.; Dingenen, R.V.; Vignati, E.; et al. Global air quality and health co-benefits of mitigating near-term climate change through methane and black carbon emission controls. *Environ. Health Perspect.* **2012**, *120*, 831–840. [CrossRef]
7. Young, C.J.; Zhou, S.; Siegel, J.A.; Kahan, T.F. Illuminating the dark side of indoor oxidants. *Environ. Sci.* **2019**, *21*, 1229–1239. [CrossRef]

8. Tatibouët, J.-M.; Valange, S.; Touati, H. Near-ambient temperature ozone decomposition kinetics on manganese oxide-based catalysts. *Appl. Catal. A Gen.* **2019**, *569*, 126–133. [CrossRef]

9. Batakliev, T.; Georgiev, V.; Anachkov, M.; Rakovsky, S.; Zaikov, G.E. Review article: Ozone decomposition. *Interdiscip. Toxicol.* **2014**, *7*, 47–49. [CrossRef]

10. Dhandapani, B.; Oyama, S.T. Review: Gas phase ozone decomposition catalysts. *Appl. Catal. B Environ.* **1997**, *11*, 129–166. [CrossRef]

11. Touati, H.; Guerin, A.; Swesi, Y.; Dupeyrat, C.B.; Philippe, R.; Meille, V.; Clacens, J.-M. Unexpected role of NOx during catalytic ozone abatement at low temperature. *Catal. Commun.* **2021**, *148*, 106163. [CrossRef]

12. Di, Q.; Dai, L.; Wang, Y.; Zanobetti, A.; Choirat, C.; Schwartz, J.D.; Dominici, F. Association of Short-Term Exposure to Air Pollution with Mortality in Older Adults. *JAMA* **2017**, *318*, 2446–2456. [CrossRef] [PubMed]

13. Wu, F.; Wang, M.; Lu, Y.; Zhang, X.; Yang, C. Catalytic removal of ozone and design of an ozone converter for the bleeding air purification of aircraft cabin. *Build. Environ.* **2017**, *115*, 25–33. [CrossRef]

14. Charpin, D.; Pairon, J.-C.; Annesi-Maesano, I.; Caillaud, D.; de Blay, F.; Dixaut, G.; Housset, B.; Meurice, J.-C.; Roussel, I.; Zmirou, D.; et al. La pollution atmosphérique et ses effets sur la santé respiratoire. Document d'experts du groupe pathologies pulmonaires professionnelles environnementales et iatrogéniques (PAPPEI) de la Société de pneumologie de langue française (SPLF). *Rev. Mal. Respir.* **2016**, *33*, 484–508. [CrossRef] [PubMed]

15. Brundrett, G. Comfort and health in commercial aircraft: A literature review. *J. R. Soc. Promot. Health* **2001**, *121*, 29–37. [CrossRef]

16. Baker, E.S.; Barratt, M.R.; Sams, C.F.; Wear, M.L. Human Response to Space Flight. In *Principles of Clinical Medicine for Space Flight*; Barratt, M., Baker, E., Pool, S., Eds.; Springer: New York, NY, USA, 2019. [CrossRef]

17. Fu, P.; Zhang, P.; Li, J. Photocatalytic degradation of low concentration formaldehyde and simultaneous elimination of ozone by-product using palladium modified TiO_2 films under UV254+185nm irradiation. *Appl. Catal. B Environ.* **2011**, *105*, 220–228. [CrossRef]

18. Fu, P.; Zhang, P.; Li, J. Simultaneous Elimination of Formaldehyde and Ozone Byproduct Using Noble Metal Modified TiO_2 Films in the Gaseous VUV. *Int. J. Photoenergy* **2012**, *2012*, 8. [CrossRef]

19. Nicolas, M.; Ndour, M.; Ka, O.; D'anna, B.; George, C. Photochemistry of Atmospheric Dust: Ozone Decomposition on Illuminated Titanium Dioxide. *Environ. Sci. Technol.* **2009**, *43*, 7437–7442. [CrossRef]

20. Ma, J.; Wang, C.; He, H. Transition metal doped cryptomelane-type manganese oxide catalysts for ozone decomposition. *Appl. Catal. B Environ.* **2017**, *201*, 503–510. [CrossRef]

21. Yu, Y.; Jia, J.; Li, K.; Huang, H.; Shrestha, R.P.; Thi, N.; Oanh, K.; Winijkul, E.; Deng, J. Activated carbon supported MnO nanoparticles for efficient ozone decomposition at room temperature. *Catal. Today* **2019**, *335*, 573–579. [CrossRef]

22. Shen, T.; Zhang, X.; Yi, K.; Lin, A.; Tong, S. Solid base Mg-doped ZnO for heterogeneous catalytic ozonation of isoniazid: Performance and mechanism. *Sci. Total Environ.* **2019**, *703*, 134983. [CrossRef] [PubMed]

23. Nawrocki, J.; Fijołek, L. Catalytic ozonation-Effect of carbon contaminants on the process of ozone decomposition. *Appl. Catal. B Environ.* **2013**, *142–143*, 307–314. [CrossRef]

24. Swesi, Y.; Gillet, A.; Guérin, A.; Zanota, M.-L.; Bornette, F.; Philippe, R.; Meille, V. Comparison of Structured Reactors for Ozone Abatement in Aircrafts at Low Temperature. *Ind. Eng. Chem. Res.* **2021**, *60*, 16739–16746. [CrossRef]

25. Xu, Z.; Yang, W.; Si, W.; Chen, J.; Peng, Y.; Li, J. A novel γ-like MnO_2 catalyst for ozone decomposition in high humidity conditions. *J. Hazar. Mater.* **2021**, *420*, 126641. [CrossRef]

26. Valdés, H.; Padilla, E.E.; Zaror, C.A. Influence of Chemical Surface Characteristics of Natural Zeolite on Catalytic Ozone Abatement. *Ozone Sci. Eng.* **2011**, *33*, 279–284. [CrossRef]

27. Lu, J.-L.; Wang, S.; Zhao, K.; Wang, T.; Ni, C.-J.; Wang, M.-Z.; Wang, S.-D. Study on catalytic performance of supported transition metal oxide catalyst for ozone decomposition. *J. Fuel Chem.* **2021**, *49*, 1014–1022. [CrossRef]

28. Jia, J.; Zhang, P.; Chen, L. Catalytic decomposition of gaseous ozone over manganese dioxides with different crystal structures. *Appl. Catal. B Environ.* **2016**, *189*, 210–218. [CrossRef]

29. Li, W.; Gibbs, G.V.; Oyama, S.T. Mechanism of Ozone Decomposition on a Manganese Oxide Catalyst. 1. In Situ Raman Spectroscopy and Ab Initio Molecular Orbital Calculations. *J. Am. Chem. Soc.* **1998**, *120*, 9041–9046. [CrossRef]

30. Jiang, C.; Zhang, P.; Zhang, B.; Li, J.; Wang, M. Facile Synthesis of Activated Carbon-supported Porous Manganese Oxide via in situ Reduction of Permanganate for Ozone Decomposition. *Ozone Sci. Eng.* **2013**, *35*, 308–315. [CrossRef]

31. Lian, Z.; Ma, J.; He, H. Decomposition of high-level ozone under high humidity over Mn–Fe catalyst: The influence of iron precursors. *Catal. Commun.* **2015**, *59*, 156–160. [CrossRef]

32. Tidahy, H.L.; Siffert, S.; Lamonier, J.-F.; Cousin, R.; Zhilinskaya, E.A.; Aboukaïs, A.; Su, B.-L.; Frère, M.; Giraudon, J.-M.; Leclercq, G. Influence of the exchanged cation in Pd/BEA and Pd/FAU zeolites for catalytic oxidation of VOCs. *Appl. Catal. B Environ.* **2007**, *70*, 377–383. [CrossRef]

33. Mendez, V.; Caps, V.; Daniele, S. Design of hybrid titania nanocrystallites as supports for gold catalysts. *Chem. Commun.* **2009**, *21*, 3116–3118. [CrossRef] [PubMed]

34. Mehri, A.; Kochkar, H.; Daniele, S.; Mendez, V.; Ghorbel, A.; Berhault, G. One-pot deposition of palladium on hybrid TiO_2 nanoparticles and catalytic applications in hydrogenation. *J. Colloid Interface Sci.* **2012**, *369*, 309–316. [CrossRef] [PubMed]

35. Klimov, O.V.; Pashigreva, A.V.; Fedotov, M.A.; Kochubey, D.I.; Chesalov, Y.A.; Bukhtiyarova, G.A.; Noskov, A.S. Co–Mo catalysts for ultra-deep HDS of diesel fuels prepared via synthesis of bimetallic surface compounds. *J. Mol. Catal. A* **2010**, *322*, 80–89. [CrossRef]

36. Comparelli, R.; Fanizza, E.; Curri, M.L.; Cozzoli, P.D.; Mascolo, G.; Passino, R.; Agostiano, A. Photocatalytic degradation of azo dyes by organic-capped anatase TiO_2 nanocrystals immobilized onto substrates. *Appl. Catal. B Environ.* **2005**, *55*, 81–91. [CrossRef]

37. Iwasa, N.; Masuda, S.; Ogawa, N.; Takezawa, N. Steam reforming of methanol over Pd/ZnO: Effect of the formation of PdZn alloys upon the Reaction. *Appl. Catal. A Gen.* **1995**, *125*, 146. [CrossRef]

38. Wu, Z.; Sheng, Z.; Liu, Y.; Wang, H.; Tang, N.; Wang, J. Characterization and activity of Pd-modified TiO_2 catalysts for photocatalytic oxidation of NO in gas phase. *J. Hazard. Mat.* **2009**, *164*, 542–548. [CrossRef]

39. Sun, Y.; Zhang, L.; Zhou, H.; Zhu, Y.; Sutter, E.; Ji, Y.; Rafailovich, M.H.; Sokolov, J.C. Seedless and Templateless Synthesis of Rectangular Palladium Nanoparticles. *Chem. Mater.* **2007**, *19*, 2065–2070. [CrossRef]

40. Kameya, T.; Urano, K. Catalytic Decomposition of Ozone Gas by a Pd Impregnated MnO_2 Catalyst. *J. Environ. Eng.* **2002**, *128*, 286–292. [CrossRef]

41. Wu, M.C.; Kelly, N.A. Clean-air catalyst system for on-road applications: II. Mechanistic studies of pollutant removal. *Appl. Catal. B Environ.* **1998**, *18*, 93–104. [CrossRef]

42. Rakitskaya, T.L.; Ennan, A.A.; Granatyuk, I.V.; Bandurko, A.Y.; Balavoine, G.G.; Geletii, Y.; Paina, V. Kinetics and mechanism of low-temperature ozone decomposition by Co-ions adsorbed on silica. *Catal. Today* **1999**, *53*, 715–723. [CrossRef]

43. Gopi, T.; Swetha, G.; Chandra Shekar, S.; Ramakrishna, C.; Saini, B.; Krishna, R.; Rao, P.V.L. Catalytic decomposition of ozone on nanostructured potassium and proton containing δ-MnO_2 catalysts. *Catal. Comm.* **2017**, *92*, 51–55. [CrossRef]

44. Spasova, I.; Nikilov, P.; Mehandjiev, D. Ozone decomposition over alumina-supported copper, manganese and copper-manganese catalysts. *Ozone Sci. Eng.* **2007**, *29*, 41–45. [CrossRef]

45. Pei, J.; Lu, Y.; Yin, X. Catalytic Decomposition of Ozone by CuO/MnO_2-Performance, Kinetics and Application Analysis. *Proc. Eng.* **2015**, *121*, 792–800. [CrossRef]

46. Subrahmanyam, C.; Bulushev, D.A.; Kiwi-Minsker, L. Dynamic behavior of activated carbon catalysts during ozone decomposition at room temperature. *Appl. Catal. B Environ.* **2005**, *61*, 98–106. [CrossRef]

47. Mehandjiev, D.; Naydenov, A.; Ivanov, G. Ozone decomposition, benzene and CO oxidation over $NiMnO_3$-ilmenite and $NiMn_2O_4$-spinel catalysts. *Appl. Catal. A Gen.* **2001**, *206*, 13–18. [CrossRef]

48. Shen, T.; Su, W.; Yang, Q.; Ni, J.; Tong, S. Synergetic mechanism for basic and acid sites of MgM_xO_y (M = Fe, Mn) double oxides in catalytic ozonation of p-hydroxybenzoic acid and acetic acid. *Appl. Catal. B Environ.* **2020**, *279*, 119346. [CrossRef]

49. Mehandjiev, D.; Naydenov, A. Ozone decomposition on α-Fe_2O_3 catalyst. *Ozone Sci. Eng.* **1992**, *14*, 277–282. [CrossRef]

50. Zhu, G.; Zhu, J.; Jiang, W.; Zhang, Z.; Wang, J.; Zhu, Y.; Zhang, Q. Surface oxygen vacancy induced-MnO_2 nanofiber for highly efficient ozone elimination. *Appl. Catal. B Environ.* **2017**, *209*, 729–737. [CrossRef]

51. Ren, C.; Zhou, L.; Shang, H.; Chen, Y. Effect of preparation method on the performance of Pd-MnOx/γ-Al_2O_3 monolithic catalysts for ground-level O_3 decomposition. *Chin. J. Catal.* **2014**, *35*, 1883–1991. [CrossRef]